# 4. Results

This section shows the results of the application of the algorithm to the test dataset relative to year 2013.

In the tuning of the algorithms we classified the precipitating pixels adopting an arbitrary rainfall rate threshold of 0.1 mm/h; however it is possible that in some conditions the radiometric signal is not suited to detect such light precipitation. Moreover an algorithm for the detection of precipitation is always a compromise between the need of detecting the lower minimum threshold of rain rate and the requirement of low detection errors in terms of both false alarms and misses. In this Section we analyze the results of the CCA algorithm for different rainfall rate thresholds ($RR_{th}$), using as ground truth for "rain" pixels TRMM-PR 2A25 product. We compare the results with those obtained from widely used screening algorithms (presented in Section 1) applying them on the same datasets used for the CCA algorithm. In particular, we have used 4 other different procedures: 1) the scattering index (Ferraro, 1997), hereafter **F97-SI**, we have calculated the scattering index (SI) over land and ocean considering also the estimated columnar water vapor from 19 GHz and 37 GHz over ocean; 2) the Polarization Corrected Temperature (PCT) algorithm from (Spencer et al., 1989) (hereafter **SGH-PCT**), we have calculated the PCT with β=0.45, considering as "rain" the pixels with PCT<255 K; 3) the AMSU/MHS screening algorithm from (Chen and Staelin, 2003), which uses differences between the 183 GHz channels and the 53.6 GHz and is applicable over each type of surface background considered in this study (hereafter **CS03**); 4) the methodology developed by Grody and Weng (2008) and used by many authors (e.g. Laviola and Levizzani (2009), (2011)), we have used the TB difference between the MHS channels at 89 GHz (or SSMIS and GMI-like 91.6 GHz) and 150 GHz as a simple mask in order to detect the scattering signal from precipitation (hereafter **GW08**). The "rain" threshold on this TB difference has been set to 5 K. Errore. L'origine riferimento non è stata trovata. summarizes the algorithms used for comparison in this study.

The results are evaluated in terms of HSS, Probability of Detection (POD) and False Alarm Ratio (FAR), defined as:

$$POD = \frac{h}{(h+m)} \qquad ; \qquad FAR = \frac{f}{(f+h)} \tag{5}$$

with the same reference to a contingency table used in Eq. (3).


## 4.1 Discussion of skill scores

Figure 3 and 4 show the results for the SSMIS (and pseudo-GMI) datasets and for the AMSU/MHS datasets respectively, for all types of surface background. All tested algorithms have higher POD for higher $RR_{th}$ because high rain rates are *usually* associated to precipitating clouds with a strong radiometric signals (except in some cases such as warm rain over land). It is worth noting, however, that the impact on the TBs in the different microwave channels depends on several factors, such as the surface background, environmental and meteorological conditions, and the microphysical structure of the cloud. FAR grows with $RR_{th}$ as well in all of the algorithms considered, as a consequence of the fact that by increasing $RR_{th}$ the size of areas considered as precipitating by the TRMM-PR is reduced, while the areas identified as "rain" by the detection algorithms are unchanged. The overall performance of the detection algorithms can be evaluated by looking at the HSS (last row in each figure).

In Figure 3, over every surface the CCA algorithm applied to SSMIS and pseudo-GMI (CCA-SSMIS and CCA-GMI) shows almost identical scores. Moreover the comparison of the scores of CCA-SSMIS on the training dataset (red crosses in Figure 4) and test dataset (continuous red line) shows a good agreement between the two, a sign of the stability of the algorithm. Over Arid Land, Vegetated Land and Coast the CCA-SSMIS performs better (i.e. higher HSS) than the other algorithms especially due to lower FAR. The SGH-PCT shows a low POD and a low FAR over all surface background. The major drawback of the SGH-PCT algorithm is that it needs to use both polarizations of the SSMIS (or pseudo-GMI) 91 GHz channels, and, therefore, it is not applicable to AMSU/MHS or other cross-track scanning radiometers. It is also worth noting that the F97-SI algorithm is not suited for detecting precipitation over desert (Arid Land) because the use of the SI leads to the misclassification of the signal deriving from the surface as precipitation (in fact it was not applied to desert background in the original work by Ferraro (1997)). Over ocean the CCA algorithms have higher POD than the others (while the FAR is comparable to CS03). Over ocean CCA-SSMIS and CCA-GMI show higher HSS than the other algorithms, except the F97-SI which has higher HSS for $RR_{th}$ larger than 0.3 mm/h. We can conclude that over ocean the CCA algorithm is more suitable to detect low precipitation rates ($RR_{th} \leq 0.2$ mm/h) than the F97-SI; however F97-SI is preferable to detect higher precipitation rates.

Figure 4 shows that the CCA-AMSU has a behavior similar to the CCA-SSMIS (CCA-GMI). No results for F97-SI and SGH-PCT are presented in this Figure because these two approaches can not be applied to the AMSU/MHS radiometers, since the 19 GHz channel and the two polarization of the 89 GHz are not available. Over Arid and Vegetated Land the CCA-AMSU performs better than the other algorithms (higher HSS, due to the significantly lower FAR). Over Coast the CCA-AMSU has skill scores very similar to the other algorithms. Finally over Ocean the CS03 and GW08 seems to work better (in terms of HSS) for high values of $RR_{th}$.

A complete and synthetic representation of the skill scores for all algorithms and but one rain rate threshold (0.1 mm/h) is provided in Figure 5 (CCA-GMI results have been omitted because identical to CCA-SSMIS scores). From this figure it is evident how the CCA algorithm both for AMSU/MHS and for SSMIS performs well in terms of HSS with respect to the other tested algorithms and how this is due to the higher POD and to the lower FAR.

## 4.2 Minimum Detectable Rate

We now want to verify how well the CCA algorithm is able to cathegorize "no rain" pixels and what is the rainfall intensity associated with misclassified pixels. Figure shows the results of a binning technique (following Ferraro and Marks (1995)) applied to the TRMM-PR rainfall rate corresponding to the CV values (Eq. 4) of each pixel. For each dataset (i.e., for SSMIS, AMSU/MHS and pseudo-GMI and for four different types of surface) the CV range of values has been divided into bins 0.2 K wide, and the mean and the standard deviation of the TRMM-PR rainfall rate corresponding to each CV value, has been calculated for each bin. Each panel shows the trend of the mean rainfall rate (and standard deviation) with the CV binned values. A thick vertical dashed line represents the CV threshold chosen for each radiometer and surface background type as a result of the CCA training (i.e, $CV_{th}$ in Eq. 5, Section 3; the values are also provided in Appendix A).

Looking at the trend of mean rain rate with CV and at the rain rate standard deviation it is evident that increasing values of CV are on average associated with increasing values of rainfall rate. All the pixels falling in the bins below $CV_{th}$ are misclassified as "no rain" and they correspond to the low rainfall values (below 0.5 mm/h for all the datasets). We have considered the minimum detectable rainfall rate for each dataset ($RR_b$) as the mean value corresponding to the $CV_{th}$. In Table 3 the values of $RR_b$ are reported and the scores of the CCA algorithm based on these thresholds are also provided. It is clear from Figure 6 and Table 1 how the CCA performs better over Vegetated Land and over Ocean for both SSMIS and AMSU, and $RR_b$ is lower over Ocean (less than 0.2 mm/h) and higher over land (around 0.3 mm/h). Over Arid Land it is possible to discriminate lower values of rain intensity (around .25 mm/h) but the strong variability in the surface emissivity leads to a higher ratio of misses (lower POD). Over Coast the results are quite different between the SSMIS and the AMSU algorithms, the $RR_b$ over Coast for the SSMIS is the highest among all the datasets (0.41 mm/h), while the irregular trend of the mean rain rate over coast for the AMSU/MHS makes the result for $RR_b$ over coast (0.24 mm/h) uncertain.

As far as the pseudo-GMI dataset, it is worth noting that it was generated from the SSMIS dataset only by discarding the channels not available in the GMI radiometer (183+-1 GHz and the 50-60 GHz band channels). Therefore the results can be representative of the performance of a CCA algorithm for the real GMI radiometer only to a certain extent, since we have considered only the instrument observation geometry (conical scanning) and some of the channels frequencies and polarizations. The presence of the 10 GHz and 166 GHz channels with both polarizations (not available on SSMIS) might have a significant impact on precipitation detection. Moreover, the differences in the resolution of the GMI and SSMIS sensors have not been considered, and this may strongly affect the results on real GMI data. It is worth noting that the almost identical results obtained for the SSMIS and pseudo-GMI datasets indicate that the inclusion of the sounding channels 183+-1 GHz and 50-60 GHz has no impact on the precipitation detection.

## 4.3 Dependence on precipitation regime

In the following subsection we have analyzed the CCA algorithm scores using the rainType flag as estimated by TRMM product 2A23. Every PR pixel has been classified into 4 main rain categories as:
1. Stratiform (rainType $\geq$ 100 and <200)
2. Convective (rainType $\geq$ 200 and <250)
3. Shallow Convective (rainType $\geq$ 250 and <300)
4. Other (rainType $\geq$ 300)

Please refer to (TRMM 2011) for details on the rainType flag definitions in the TRMM-PR product 2A23. In the test datasets this information was downscaled to the SSMIS and MHS nominal resolutions, i.e. the fraction of PR pixels categorized as one of the main rain category within each SSMIS and AMSU/MHS pixel has been calculated. This quantity has been compared to the fraction of precipitating pixels as observed by PR (considering a 0.1 mm/h threshold). Each pixel in the SSMIS-PR and AMSU/MHS-PR datasets has been classified as mainly Convective if at least 50% of the precipitating part of the pixel was Convective. The same criterion was adopted for each rain category. If a pixel was classified as precipitating with no predominance of any of the main rain type class, it was flagged as Mixed.

Table 4 shows the POD score for each rain type class and for each surface background. Moreover Table 5 shows the POD calculated as a function of the fraction of precipitation in the pixel (for all surface background classes together). It is clear from Tables 4-5 how the CCA algorithm detects very well Convective and Stratiform precipitation while it is almost insensitive to Shallow precipitation over land and coast, while it gives medium performances (between .30 and .58) for Other and Mixed types. However, from Table 5 it is evident that the detection capability of precipitation grows with the fraction of precipitation within the SSMIS and MHS pixels. This results indicate that the non uniform beam filling effect can have a significant impact on the detection of the precipitation, and the impact depends on the predominant type of precipitation within each pixel (i.e, the most significant impact for shallow precipitation, the least significant for stratiform precipitation, and quite significant for convective precipitation).

Table 6 shows the results for the false alarms. In detail, the first column shows the FAR scores for each surface type, while the other columns show the percentage of false alarms counts (for each surface type) for three classes of rain/no rain conditions based on the 2A23 rainFlag. The three classes are:

1. Low rain: SSMIS or AMSU/MHS pixels classified as "rain certain" (rainFlag equals to 20). For this class CCA false alarms refer to PR downscaled rain rates less than 0.1 mm/h.
2. Potential Rain: SSMIS or AMSU/MHS pixels classified as "rain possible" or "probable" (rainFlag between 10-15). For this class false alarms refer to PR downscaled rain rates equal to 0 mm/h. This class includes very weak echos (possibly noise) and not precipitating clouds.
3. No rain: SSMIS or AMSU/MHS pixels classified as "no rain" " (rainFlag equals to 0).

It is clear from Table 6 how only a relatively small percentage of the false alarms are related to "no rain" pixels (especially for AMSU/MHS) and a not negligible part of the false alarms is associated with PR observations with low rain rates.
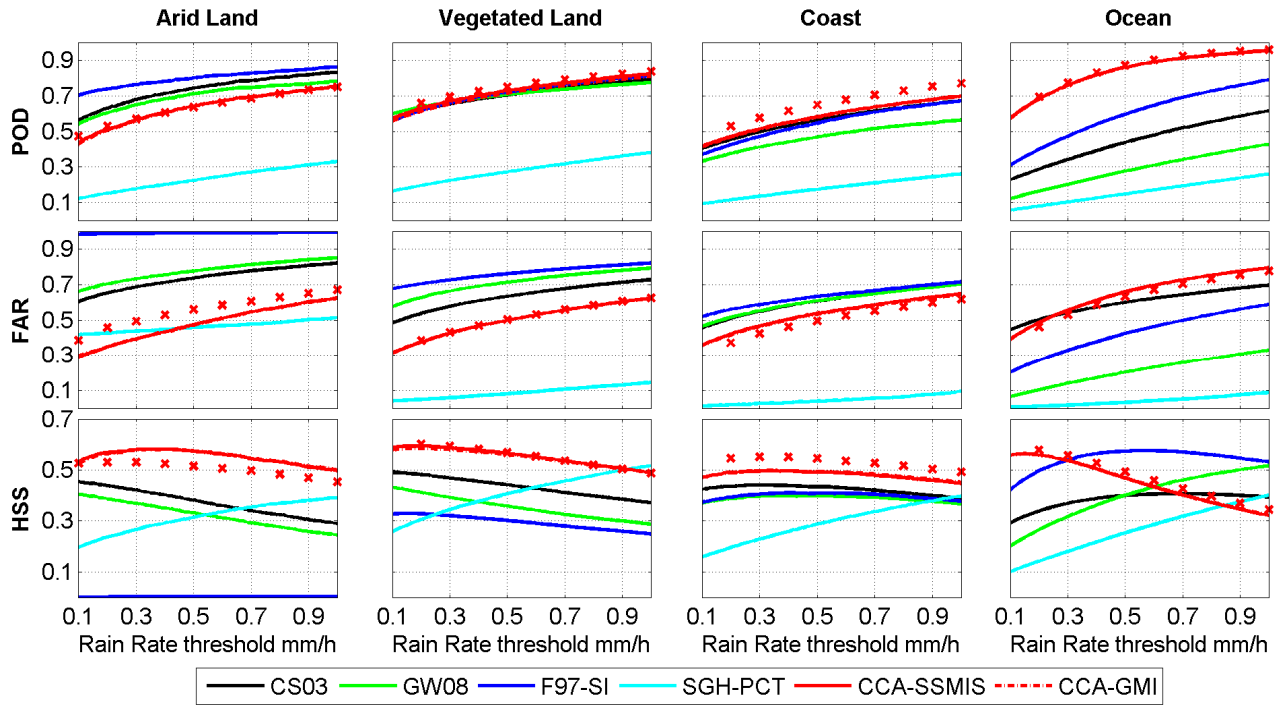
# Figures in Section 4



Figure 3 Comparison of the CCA-SSMIS and CCA-GMI algorithm with other similar algorithm for the detection of precipitation using as ground truth for the precipitating pixels the PR- rain rate with a variable threshold (represented in the x axis). The results are shown in 4 columns of panels (one for each surface type) in terms of POD (upper row of panels), FAR (middle row) and HSS (lower row). The scales are the same for every plot. Solid lines show the statistical indexes resulting from the application of a screening algorithm to the test dataset (year 2013), Red crosses are the result of the application of the SSMIS-CCA algorithm to the training dataset (years 2011-2012).
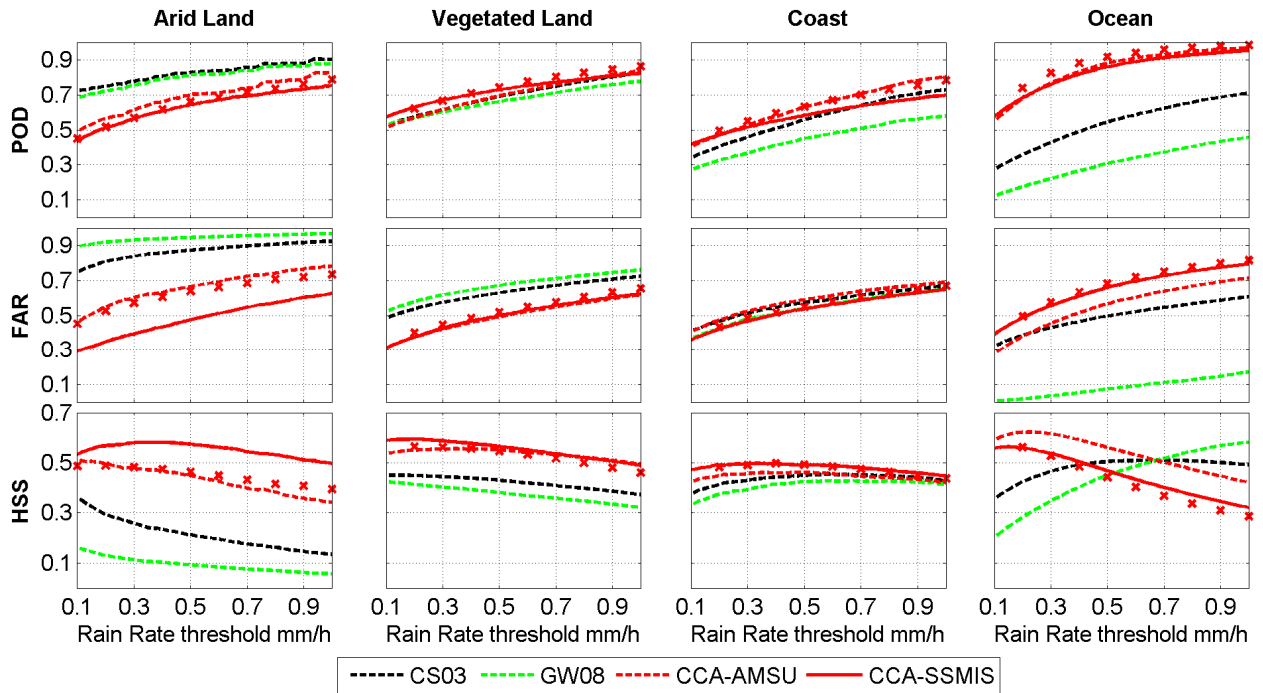
Figure 4 Same as Fig. 3 but for the AMSU/MHS dataset. The CCA-SSMIS (red solid curve) (results of the CCA algorithm applied to SSMIS test dataset shown in Fig. 3



Figure ),are shown here for comparison. Red crosses are the result of the application of the CCA-AMSU algorithm to the training dataset (years 2011-2012).

**Figure 5**: Skill score comparison of the CCA algorithm with other precipitation detection algorithms with rain/no-rain threshold ("truth" from PR 2A25) equal to 0.1 mm/h



Figure 6: Binning analysis of the rain rate intensity against CV values: mean (continuous black line) and standard deviation (error bars) of rain rates inside an interval of CV bins (as large as 0.2 K) are

shown. The vertical dashed line represents the CV threshold (CVth) chosen for each radiometer and surface background combination.
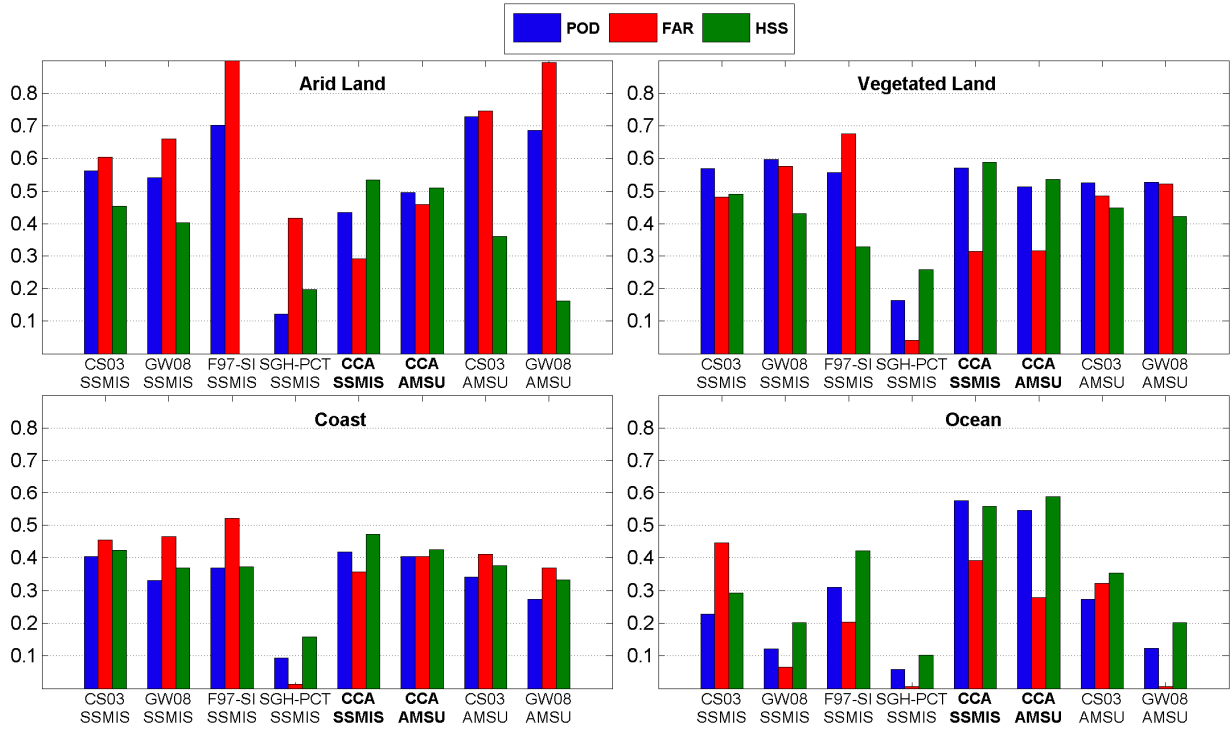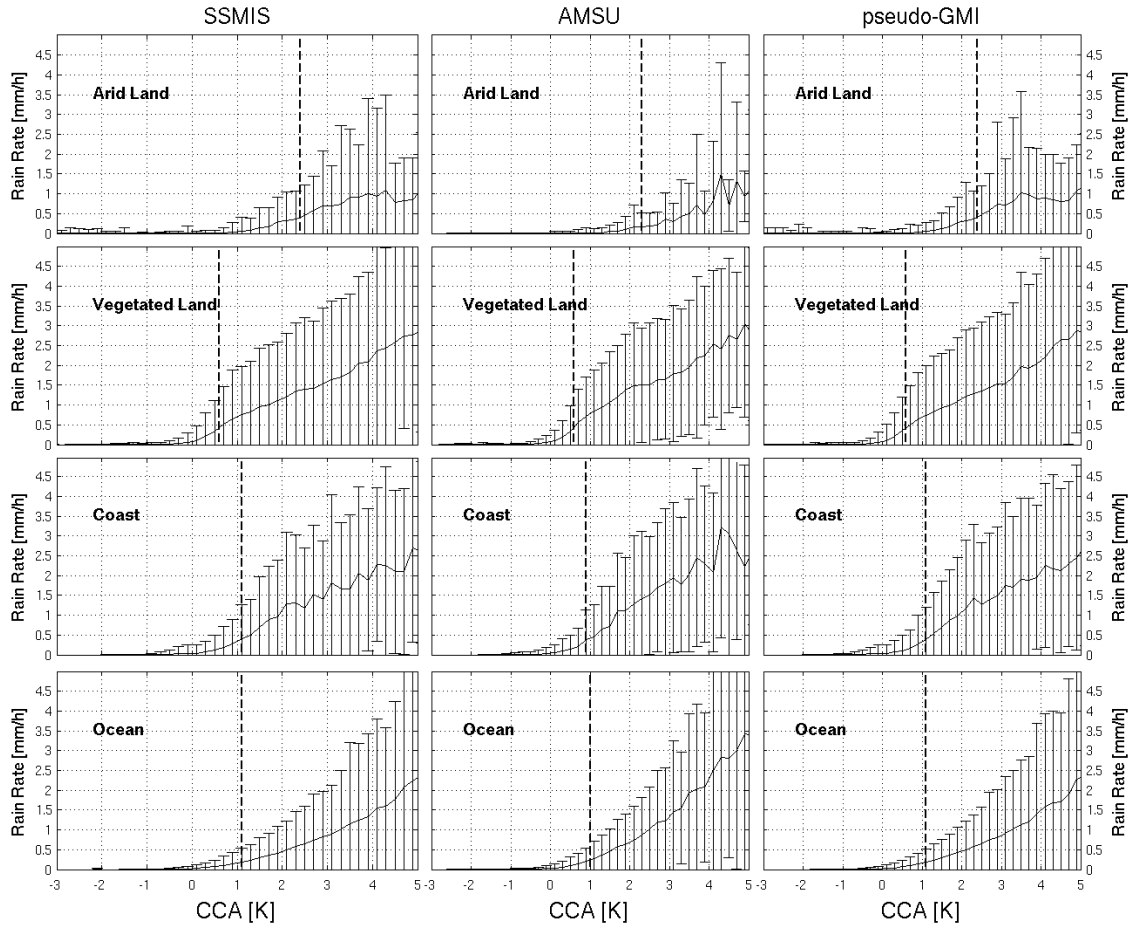
## Tables in Section 4

**Table 1** Value of the mean rain rate corresponding to the CCA threshold set for every radiometer and surface background combination. Values in bold refer to the test dataset while the italics values refer to the training dataset.

| | SSMIS | | | | AMSU/MHS | | | | GMI | | | |
|---|---|---|---|---|---|---|---|---|---|---|---|---|
| | Arid Land | Veg. Land | Coast | Ocean | Arid Land | Veg. Land | Coast | Ocean | Arid Land | Veg. Land | Coast | Ocean |
| $RR_{th}$ (mm/h) | **0.25** | **0.35** | **0.41** | **0.18** | **0.26** | **0.31** | **0.24** | **0.14** | **0.33** | **0.38** | **0.40** | **0.18** |
| POD ($RR_{th}$) | *0.57* | *0.74* | *0.62* | *0.68* | *0.56* | *0.73* | *0.61* | *0.71* | *0.60* | *0.73* | *0.62* | *0.67* |
| | **0.61** | **0.71** | **0.55** | **0.67** | **0.55** | **0.69** | **0.57** | **0.72** | **0.60** | **0.71** | **0.54** | **0.67** |
| FAR ($RR_{th}$) | *0.50* | *0.49* | *0.47* | *0.45* | *0.55* | *0.52* | *0.57* | *0.47* | *0.51* | *0.50* | *0.47* | *0.44* |
| | **0.44** | **0.49** | **0.50** | **0.47** | **0.52** | **0.51** | **0.58** | **0.43** | **0.44** | **0.50** | **0.50** | **0.47** |
| HSS ($RR_{th}$) | *0.53* | *0.57* | *0.55* | *0.58* | *0.49* | *0.53* | *0.45* | *0.56* | *0.53* | *0.56* | *0.54* | *0.58* |
| | **0.58** | **0.56** | **0.50** | **0.56** | **0.50** | **0.53** | **0.42** | **0.61** | **0.58** | **0.55** | **0.50** | **0.56** |

**Table 4.** Probability of Detection scores classified by surface background and Rain Type

| | | **POD** | | | | |
|---|---|---|---|---|---|---|
| | | **Convective** | **Stratiform** | **Shallow** | **Other** | **Mixed** |
| **SSMIS** | Arid Land | **0.61** | **0.68** | **-** | **0.30** | **0.33** |
| | Veg. Land | **0.76** | **0.84** | **0.08** | **0.55** | **0.48** |
| | Coast | **0.68** | **0.82** | **0.09** | **0.39** | **0.36** |
| | Ocean | **0.84** | **0.93** | **0.42** | **0.48** | **0.55** |
| **AMSU/MHS** | Arid Land | **0.73\*** | **0.77** | **-** | **0.44\*** | **0.33\*** |
| | Veg. Land | **0.76** | **0.84** | **0.07\*** | **0.45** | **0.47** |
| | Coast | **0.75** | **0.87** | **0.09** | **0.30** | **0.38** |
| | Ocean | **0.89** | **0.96** | **0.40** | **0.38** | **0.58** |

**\*sample 100-500 pixels.**

**Table 5.** Probability of Detection scores classified by Rain Type and percentage of precipitation in the pixel. No results are provided for samples with less than 100 pixels.

| POD with fraction of precipitation | | | | | |
|---|---|---|---|---|---|
| | **Fraction of precip.** | **Convective** | **Stratiform** | **Shallow Conv** | **Other** | **Mixed** |
| | >0.1 | 0.75 | 0.87 | 0.38 | 0.47 | 0.53 |
| | >0.2 | 0.77 | 0.88 | 0.44 | 0.47 | 0.53 |
| | >0.3 | 0.79 | 0.88 | 0.47 | 0.47 | 0.57 |
| | >0.4 | 0.81 | 0.89 | 0.49 | 0.49 | 0.62 |
| SSMIS | >0.5 | 0.82 | 0.91 | 0.51 | 0.56 | 0.69 |
| | >0.6 | 0.84 | 0.92 | 0.54 | 0.59 | 0.71 |
| | >0.7 | 0.84 | 0.93 | 0.61 | 0.57 | 0.81 |
| | >0.8 | 0.88 | 0.95 | 0.68 | 0.63 | 0.90 |
| | >0.9 | 0.89 | 0.96 | 0.71 | 0.70 | 0.92 |
| | >0.1 | 0.79 | 0.89 | 0.28 | 0.40 | 0.52 |
| | >0.2 | 0.81 | 0.90 | 0.32 | 0.41 | 0.57 |
| | >0.3 | 0.84 | 0.91 | 0.36 | 0.45 | 0.64 |
| | >0.4 | 0.87 | 0.93 | 0.44 | 0.57 | 0.70 |
| AMSU/MHS | >0.5 | 0.91 | 0.95 | 0.57 | 0.73 | 0.81 |
| | >0.6 | 0.93 | 0.96 | 0.59 | 0.81 | 0.88 |
| | >0.7 | 0.97 | 0.97 | 0.70* | 0.84 | 0.94 |
| | >0.8 | 0.99 | 0.98 | 0.75* | 0.88* | 0.98 |
| | >0.9 | 1.00 | 0.99 | - | - | 1.00 |

**\*sample 100-500 pixels.**

**Table 6.** False Alarm Ratio scores classified by Surface and Rain Flag. Percentages represents the fraction of false alarms counts for a given surface type and rainFlag w.r.t the total number of false alarms for each surface type.

| False Alarms | | | | | |
|---|---|---|---|---|---|
| | | **Total FAR** | **Low Rain %** | **Potential Rain %** | **No-Rain %** |
| | Arid Land | 0.29 | 29.03% | 52.23% | 18.74% |
| SSMIS | Veg. Land | 0.31 | 27.15% | 49.25% | 23.60% |
| | Coast | 0.36 | 27.03% | 45.95% | 27.03% |
| | Ocean | 0.39 | 29.58% | 35.07% | 35.35% |
| | Arid Land | 0.46 | 39.27% | 57.58% | 3.16% |
| AMSU/MHS | Veg. Land | 0.32 | 48.75% | 45.76% | 5.49% |
| | Coast | 0.40 | 55.16% | 38.57% | 6.27% |
| | Ocean | 0.28 | 59.57% | 33.77% | 6.66% |